Journal of Materials Science: Materials in Electronics (2018) 29:18020–18029
https://doi.org/10.1007/s10854-018-9988-x

REVIEW

Microwave-hydrothermal synthesis of $Y_3Fe_{3.35}Al_{1.65}O_{12}$ nanoparticles for magneto-hyperthermia application

E. Borsari[1] · B. G. G. Freire[1] · F. G. Garcia[2] · M. S. Silva[2] · C. C. Silva[1] · A. Z. Simões[1]

Received: 19 January 2018 / Accepted: 1 September 2018 / Published online: 5 September 2018

Abstract
Crystalline aluminum substituted yttrium iron garnet nanoparticles $Y_3Fe_{3.35}Al_{1.65}O_{12}$ (YIG) was synthesized by hydrothermal microwave synthesis at 140 °C with soaking times ranging from 15 to 60 min. X-ray diffraction confirmed the single-phase YIG nanoparticles excluding the presence of any other phases in the reaction products. The Raman spectra revealed that the largest soaking time provides greater energy crystallization causing changes of lattice vibration and a certain degree of disorder in the crystal lattice. Field emission gun-scanning electron microscopy and high resolution transmission electronic microscopic revealed a homogeneous size distribution of nanometric YIG powders with agglomerated particles. Magnetic measurements were achieved by using a vibrating-sample magnetometer unit. YIG nanoparticles have great potential in magneto-hyperthermia application once in vivo applications magnetic induction heating ferromagnetic compounds generate heat in AC magnetic fields.

1 Introduction

Magnetic hyperthermia (MH) is a promising therapeutic method based on the use of magnetic nanoparticles (MNPs). MH is a two-step procedure: MNPs are first injected into the tumor; the patient is then immersed in an alternating magnetic field with a frequency f and an amplitude $\mu_0 H_{max}$ appropriately chosen. Due to the excitation of the MNPs, the temperature of the tumor rises. This temperature increase improves the efficiency of chemotherapy (T = 42–45 °C) or can even directly kill the tumor cells by necrosis (T > 50 °C) [1–6]. Therefore, the ideal mechanism for a proper use in hyperthermia must be capable of heating the cancer site affecting the less possible the surrounding healthy tissues. Gilchrist et al. [5] suggested that the selectivity required can be achieved through a powdered magnetic material with controlled particle size which must be one micron or less in diameter. Hence, the magnetic particles can be guided or localized in a specific target through an external magnetic field [6]. Kumar's recent review [7] pointed out many types of magnetic materials that have been studied for their hyperthermia potential, most of them iron oxide-based materials. As known, the iron-containing oxide phases with $A_3B_5O_{12}$ cubic garnet structure possess unique magnetic, magneto-optical, thermal, electrical and mechanical properties, such as ferrimagnetism, excellent creep, high thermal conductivity, high electrical resistivity, moderate thermal expansion coefficients, radiation damage resistance, energy-transfer efficiency and controllable magnetization saturation [8]. Yttrium iron garnets (YIG), $Y_3Fe_5O_{12}$, belongs to this class of materials. Since their discovery in 1956 by Bertaut and Forrat [9], YIG have attracted attention due to their interesting properties, as low dielectric loss, narrow resonance linewidth in microwave region and good saturated magnetization value [10], and as an important material in optical communication and magneto-optical devices [8–12]. YIG crystallizes in cubic structure, space group Ia3d, with eight molecules in a unit cell of lattice constant a = 12.376 ± 0.004 Å [12]. There are three sublattices: tetrahedral (d), octahedral (a) and dodecahedral (c). They are surrounded by four, six and eight oxygen ions, respectively. The unit formula can be written as $Y_3Fe_2(FeO_4)_3$ and yttrium ions occupy 24c (dodecahedral) sites, two iron ions occupy 16a (octahedral) sites and the other three iron ions occupy 24d (tetrahedral) sites. The only magnetic ion in YIG is

✉ E. Borsari
elidesborsari@hotmail.com

✉ A. Z. Simões
alezipo@yahoo.com

[1] Faculty of Engineering of Guaratinguetá, São Paulo State University - UNESP, Guaratinguetá, SP, Brazil

[2] Physics and Chemistry Institute, Federal University of Itajubá - UNIFEI, Itajubá, MG, Brazil

Fe^{3+}. A magnetic moment of 5 μ_B per formula unit results from antiferromagnetic superexchange interaction between these Fe^{3+} ions in octahedral and tetrahedral sites through the intervening O^{2-} ions [8, 12, 13]. Akhtar et al. studies [14] showed that magnetic properties (such as remanence and saturation) depend on particle size, magnetic dilution and superexchange interaction of the YIG ferrites. Although YIG high saturated magnetization value is significant for hyperthermia, its controllable Curie temperature (or Curie point) is an equally important property. Above Curie temperature ferromagnetic material becomes paramagnetic. When exposed to an external magnetic field, YIG generates heat due to both Neel and Brown relaxation [15]. Once these particles reach Curie temperature, no heat is generated preventing overheating and damaging human tissues. The substitution of metal ions in the ferrite structure can affect the magnetic, electrical and dielectric properties of ferrites [15]. As Grasset et al. demonstrated [16], aluminum substituted YIG ($Y_3Fe_{5-x}Al_xO_{12}$, $0 \le x \le 2$) decreases Curie point near body temperature by adjusting Fe/Al ratio, allowing such particles self-regulated and safe-guarded for hyperthermia applications. Several methods has been described in literature for obtaining YIG, such as the mechanochemical method [13], solid state reaction [17], citrate sol–gel [18], microwave-induced combustion [19], hydroxide coprecipitation [20], coprecipitation in microemulsion [21], metal alkoxides hydrolysis [22], glycothermal synthesis [23] and glass-crystallization [24]. In microwave hydrothermal synthesis is necessary high pressure to maintain a phase in solution under high temperatures. This phase in solution provides the mass transport, increasing the kinetics of phase transformation, thus resulting in particles with high crystallinity. In this paper, microwave hydrothermal synthesis was employed due the possibility to obtain high purity powders with close particles distribution at low temperatures resulting in a cheap process. This technique is faster and less expensive comparing to others methods [25–30]. Nasaba et al. [31] employed sonochemical synthesis of terbium tungstate (TWNPs) for high power supercapacitors with enhanced energy densities. The prepared nanoparticles were evaluated through scanning electron microscopy (SEM), thermogravimetric analysis (TGA), X-ray diffraction (XRD), Fourier transform infrared spectroscopy (FT-IR) and UV–Vis Spectroscopy. The optimal products were further characterized in terms of their electrochemical properties using conventional and continuous cyclic voltammetry (CV, and CCV), galvanostatic charge/discharge technique, and electrochemical impedance spectroscopy (EIS). The CV studies indicated the TWNPs have specific capacitance (SC) values of 336 and 205 Fg^{-1} at 1 and 200 mV s^{-1}, and galvanostatic charge–discharge tests revealed the SC of the TWNP-based electrodes to be 300 Fg^{-1} at 1 Ag^{-1}. Also, continuous cyclic voltammetry measurements have shown a capacitance retention value of 95.3% after applying 4000 potential cycles [32]. Arania et al. [33] using the same procedure, have obtained $YbVO_4/CuWO_4$ nanocomposites and the influence of parameters such as time, power, temperature and solvent and their dependence on size, morphology and uniformity were compared. The effect of the ultrasonic radiation on the photocatalytic behavior of $YbVO_4/CuWO_4$ shows that methylene blue pollutant was about 100% destructed with ultrasonic wave and 61% in the absence of ultrasonic radiation. Ahmadi et al. [34] investigated the $YbVO_4/NiWO_4$ nanocomposites synthesized by simple and new co-precipitation method. Photocatalytic, optical, and magnetic properties of the products were examined in the presence of different dyes such as methylene blue, methyl-violet, methyl orange, and rhodamine B. The highest and lowest percentages of dyes degradated were obtained for rhodamine B and phenol red dyes with 98% and 65%, respectively. Also, Niasari et collaborators [35] synthesized by the sol–gel method $CdTiO_3$ nanoparticles through reaction between $Cd(CH_3COO)_2{\cdot}2H_2O$, $Ti(OC_4H_9)_4$, trimesic acid as a new chelating agent and ethanol as solvent. It was found that temperature and time of calcination, pH and the solvent of reaction are important in the formation of $CdTiO_3$ nanoparticles. In this research, $Y_3Fe_{3.35}Al_{1.65}O_{12}$ composition was investigated because presents a transition phase (T_c) or Curie point close to the capable of heating the cancer site affecting the less possible the surrounding healthy tissues at around ($T_c = 42$–45 °C).

2 Experimental procedure

2.1 Synthesis of nanoparticles

Reactants were provided by Aldrich: $Y(NO_3)_3{\cdot}6H_2O$ (99.9%), $AlC_5H_5O_7$ (99.9%) and $FeC_6H_5O_7{\cdot}NH_4OH$ (99.5%) by Merck. All reagents were weighted according to the previous $Y_3Fe_{3.35}Al_{1.65}O_{12}$ stoichiometry. The solution was obtained dissolving yttrium nitrate hexahydrate with drops of nitric acid, ammonium iron(III) citrate and aluminum citrate in water by constant mixing at 90 °C. Afterwards, pH of solution was measured and is around three. The resulted solution was transferred into a sealed Teflon autoclave and placed in a hydrothermal microwave (2.45 GHz, maximum power of 800 W). The reactional system was heat treated at 140 °C for different soaking times (15, 30 and 60 min) with a heating rate fixed at 10 °C min^{-1}. The pressure in the sealed autoclave was stabilized at 1.2 atm. The autoclave was cooled to the room temperature naturally. Polycrystalline $Y_3Fe_{3.35}Al_{1.65}O_{12}$ (YIG) nanoparticles were collected and washed with water several times and then dried at 80 °C in an oven.

2.2 Structural, morphological and physical characterization of nanoparticles

The obtained nanoparticles were characterized by X-ray powder diffraction (XRD) using a (Rigaku-DMax/2500PC, Japan) with Cu-Kα radiation (λ = 1.5406 Å) in the 2θ range from 10° to 75° with 0.2° min^{-1}. Raman spectra were collected (Bruker RFS-100/S Raman spectrometer with Fourier transform). A 1064 nm YAG laser was used as the excitation source, and its power was kept at 150 mW. The FT-IR spectra were recorded with a Bruker Equinox-55 instrument and allows to determine contaminants from the synthesis and adsorbed at the powder surface. The morphology of as-prepared samples was observed using a high resolution field–emission gun-scanning electron microscopy (FEG-SEM) (Supra 35-VP, Carl Zeiss, Germany). Specimens for TEM were obtained by drying droplets of as-prepared samples from an ethanolic dispersion which had been sonicated for 5 min onto 300 mesh Cu grids. TEM images were then taken at an accelerating voltage of 200 kV on a Philips model CM 200 instrument. To measure the dc magnetic field, a Hall probe was employed. Magnetization measurements taken at room temperature were done by using a Vibrating-Sample Magnetometer (VSM) from Quantum Design™. The Mossbauer spectra were recorded at room temperature on a Wissel spectrometer equipped with $^{57}Co/Rh$ source. After sintering the disks were polished to 1 mm in thickness and characterized by means of electrical measurements. Gold electrodes were applied by evaporation through a sputtering system in a polished surface of sintered discs. $Y_3Fe_{3.35}Al_{1.65}O_{12}$ powders were pressed into pellets and sintered at an appropriate temperature of 1000 °C for 1 h. The samples were polished to 1.0 mm in thickness. Measurements of the capacitance as a function of temperature at 10 kHz were performed. From the capacitance dependence temperature curves, the Curie temperature was determined in an impedance analyser, model 4192 of HP.

3 Results and discussion

Aluminum substituted YIG with formula $Y_3Fe_{3.35}Al_{1.65}O_{12}$ was synthesized by microwave hydrothermal synthesis at different soaking times with a constant pH, pressure and temperature. Independent of the soaking time employed, the diffraction patterns reveals that yttrium aluminum iron garnet appears as a single phased at 140 °C. The Bragg peaks are in agreement to what is found in literature [19], proving that the particles are pure phase. XRD patterns reveal that the structure of powders is *bcc* and the garnet phase has been obtained (Fig. 1). No shift of diffraction lines of Bragg angles with increasing soaking time was observed implying that the crystal surfaces were not damaged at different

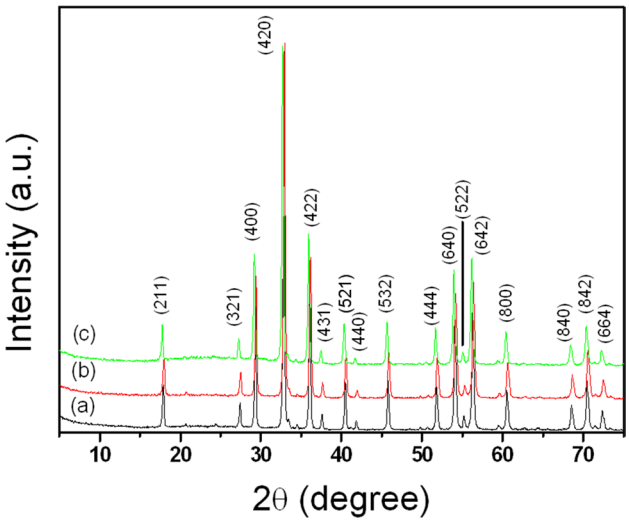

Fig. 1 X-ray diffraction pattern of $Y_3Fe_{3.35}Al_{1.65}O_{12}$ powders synthesized at 140 °C for 15, 30 and 60 min through microwave hydrothermal synthesis method

two tetha positions. In the soaking time range evaluated, no traces of impurities was formed and the formation of pure YIG was demonstrated. As the soaking time enhances, the YIG crystal growth is established. The garnet structure is formed instead other non-stoichiometry compounds due the fact that the raw salts precursors of yttrium, aluminum and iron were easily dissociable in few millilitres of water treated with acid producing a highly exothermic reaction. In the HTMW synthesis, the conversion of the nonstoichiometry compound to oxide is quite fast to the effect of energetic radiations assisting the transformation. In the oxidizing atmosphere, dehydration occurs.

Figure 2 shows the Raman spectra of $Y_3Fe_{3.35}Al_{1.65}O_{12}$ polycrystalline powders with different soaking times. It is known there is no structural difference in crystal of these powders according to XRD analysis. However, Raman spectrum reveals some evident changes of vibration frequencies of molecules as the soaking time increases. Nine sharp bands that are associated with internal vibrations modes of FeO_4 molecular group were evidenced. Below 300 cm^{-1} these modes are characterized as translational mode (T) of Y^{3+}, $[FeO4]^{5-}$ and or $[FeO6]^{9-}$ [31, 32] and the modes above 300 cm^{-1} are assigned to vibrational modes internal corresponding to T_{2g}, E_g, and A_{1g} [31, 32]. The main differences in the observed spectra is presented in the 400–600 cm^{-1} which clearly observed a reduction in relative intensity of these bands relative to the band E_g mode at 620 cm^{-1}. A gaussian deconvolution evidenced the overlap of the A_{1g}, E_g and T_{2g} modes. As the soaking time increases the E_g and T_{2g} modes is more pronounced while the A_{1g} mode is suppressed. The appearance of such modes demonstrates that the network structure has suffered a distortion in the

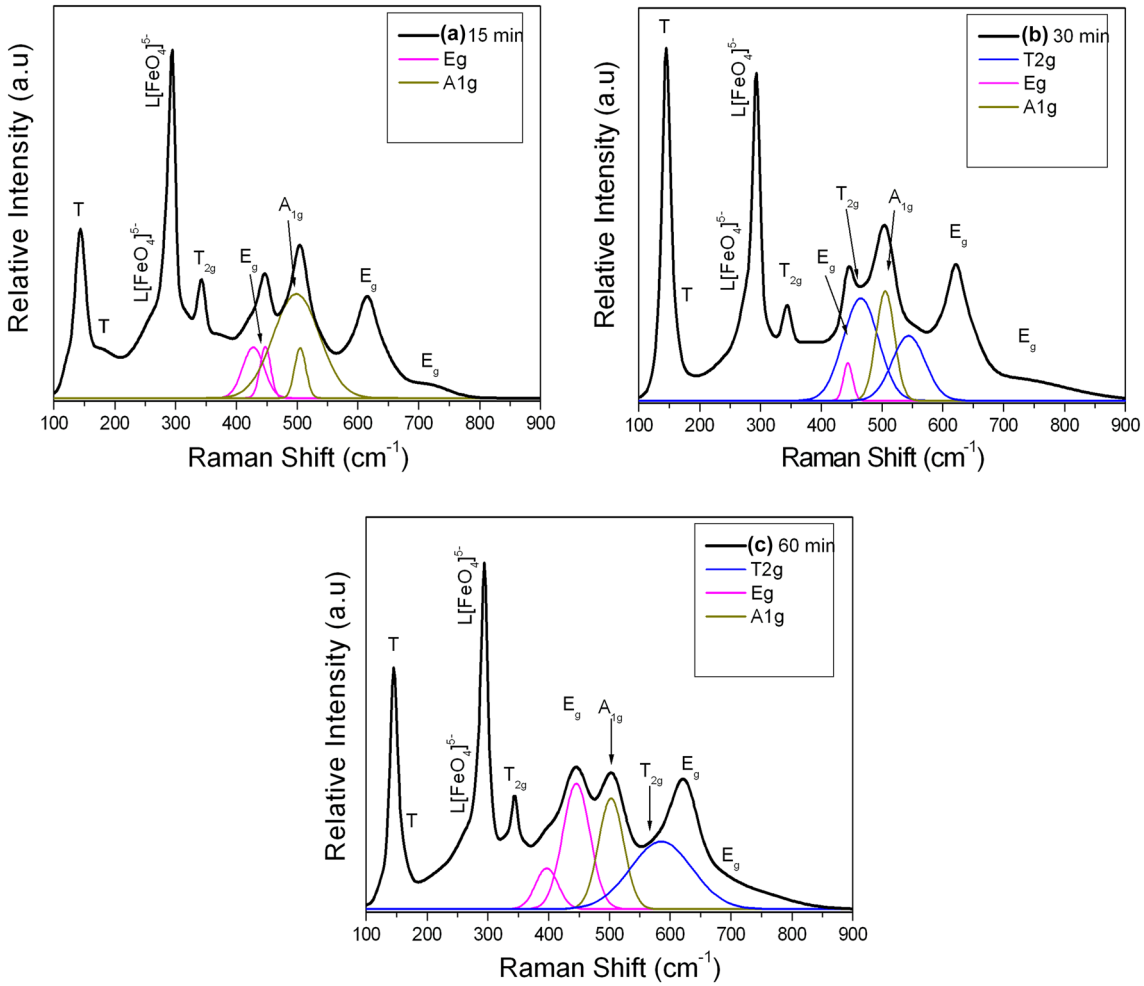

Fig. 2 Raman spectra of $Y_3Fe_{3.35}Al_{1.65}O_{12}$ powders synthesized at 140 °C through microwave hydrothermal synthesis method with soaking times of: **a** 15, **b** 30 and **c** 60 min

symmetrical axis with respect to the A_{1g} axis and so bending or stretching in the crystalline lattice is distorted in two-dimensional form (E_g) and three dimensional (T_{2g}). This is because the largest soaking time provides greater energy crystallization, causing anisotropy in the structural growth at short range and thus causing a certain degree of disorder in the crystal lattice. Another contribution comes from the fact that YIG crystal can be doped leading to several displacement of aluminum by iron as the soaking time increases. In the YIG crystal, there are 16 octahedral A lattices, each with six coordinating oxygen ions and 24 tetrahedral D lattices, each with four coordinating oxygen ions. Fe^{3+} ion displacement may take place in either one of these lattices. It may be reasonably assumed that ion displacement in these lattices may be sequential. That is, one group may start after the other finishes. Since the Al^{3+} induced vibrational modes give rise to higher mode intensities, the remaining spectral signals may, therefore, be attributed to those lattices in which their Al^{3+} ions are not yet displaced.

FT-IR spectra for all soaking times are shown in Fig. 3. The presence of multiple bonds in the $Y_3Fe_{3.35}Al_{1.65}O_{12}$ powders can be noticed. All soaking times analyzed presented O–H bonds stretching from 3200 to 3600 cm^{-1} and a vibration band at1680 cm^{-1} which is associated to the deformation of O–H bonds. These bands can be attributed to water adsorbed at the powder surface when the sample was in contact with the environment. Wavenumbers ranging from 825 to 930 cm^{-1} represents axial strain of C–O bonds in carbonates while such bands from 545 to 680 cm^{-1} are characteristic of metal–oxygen bonds. Unlike previous studies [24], FT-IR spectra show very weak bands characteristic of carbonates (1400 and 1520 cm^{-1}). The band at 2339 cm^{-1} was previously assigned by Vaqueiro et al. to atmospheric CO_2 [24]. For all samples, wavenumbers ranging from 400 to 700 cm^{-1} represents the presence of oxygen–metal phase.

FEG-SEM was used to evaluate morphology of $Y_3Fe_{3.35}Al_{1.65}O_{12}$ nanoparticles, Fig. 4a–c. All samples were prepared through microwave hydrothermal synthesis

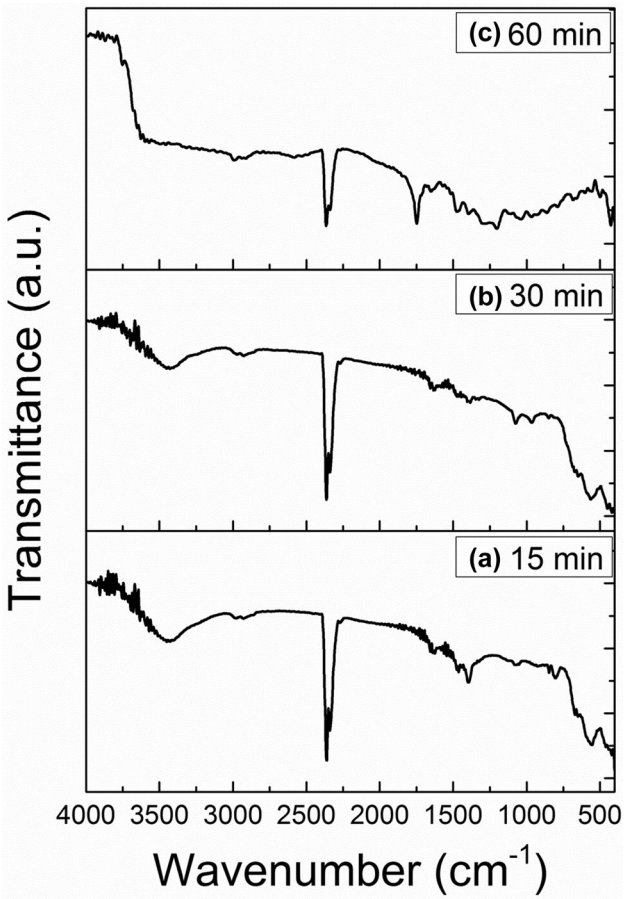

Fig. 3 FT-IR of $Y_3Fe_{3.35}Al_{1.65}O_{12}$ powders synthesized at 140 °C through microwave hydrothermal synthesis method with soaking times of: a 15, b 30 and c 60 min

with different soaking times (15, 30 and 60 min) at 140 °C. The particle size reached approximately 20–60 nm with some agglomerates. The enhancement of the soaking time apparently has not affected initial characteristic of agglomerates which is stronger expressed as blocks of irregular form. After hydrothermal treatment to obtain $Y_3Fe_{3.35}Al_{1.65}O_{12}$ in aqueous solution at lower soaking times, the Van der Waal's force derived for the –OH ligand precursor caused higher agglomeration degree. The sizes of crystals become larger with soaking time increasing, and crystal quality gradually becomes better with increasing size. On the other hand, powders' morphology has not changed, nevertheless, whereas time increases. At higher soaking times, some heterogeneities are formed on the powders' surface although the aggregation between the particles decreases and monodispersed particles are observed. Moreover, the distribution in size seemed to be homogeneous and the shape appeared to be in blocks. During the hydrothermal crystallization many factors influencing the formation of products are involved, such as alkalinity, soaking time, crystallization temperature. As the temperature and pressure conditions are carefully maintained during the experiments, neither etching of YIG crystals nor the formation of a second phase is observed. Therefore, in the hydrothermal process the dissolution and crystallization process continued in supersaturated fluid in such a way that the system was self-stabilizing preventing the formation of ionic complexes. This inhibits the growth of YIG crystallites and limit their sizes to the nanometric range.

High-resolution transmission electron microscopy (HRTEM) was used to evaluate the particle shape and size of the garnet structure. $Y_3Fe_{3.35}Al_{1.65}O_{12}$ with good crystallinity has been achieved at the soaking time of 30 min. The micrographs revealed that the average grain size varies between 40 and 70 nm, (Fig. 5a–c). The small size of the particles synthesized at a lower soaking time can be explained as follows: a large number of nuclei is formed in the solution at the beginning of the reaction. As the reaction proceeds in a very dilute solution, there is not enough reactant left for the growth of the particles and as a consequence, the particles do not grow beyond 40 nm. As the soaking time reaches 60 min, the large agglomerates disappeared and became smaller isometric ones, thus the particle size maximum increased sharply attaining a value of 70 nm. As already seen in FEG-SEM, no obvious change in the morphology under HTMW conditions is attained. The particles agglomeration seen in HRTEM image could be due to magnetic nature of the single-domain particles. In general, in the microwave assisted process, the smaller particles usually owe higher surface energy that makes them more easily to aggregate together once the microwave field is a union of magnetic field and electric field changing their direction at a frequency of 2.45 GHz.

M–H loops of $Y_3Fe_{3.35}Al_{1.65}O_{12}$ powders as a function of different soaking times is displayed in Fig. 6. Magnetic behavior might be attributed to the arrangement of magnetic moments within the crystals and the effect of high internal field of samples causing ferromagnetism. This may be Intern field can be generated due to asymmetric distribution of loaded oxygen vacancies. This effect induces complexes dipoles alignment and asymmetric distribution of loaded oxygen vacancies, i.e.; oxygen vacancies loaded positively next to negative electrode that holds electrons next to positive electrode. Magnetic curve's behavior indicates that Al and Fe distribution in different soaking times might be attributed to difference in morphology, defects density, and phase composition. The presence of non-collinear magnetic structure in the magnetic sublattices can be due the triangular spins configurations or spiral configurations. Although remaining magnetization is greater for crystalline powders obtained at 15 min, greater disordered structure suggests deeper studies related to formation of phase in short and medium interatomic distances (Table 1). Also, the longest

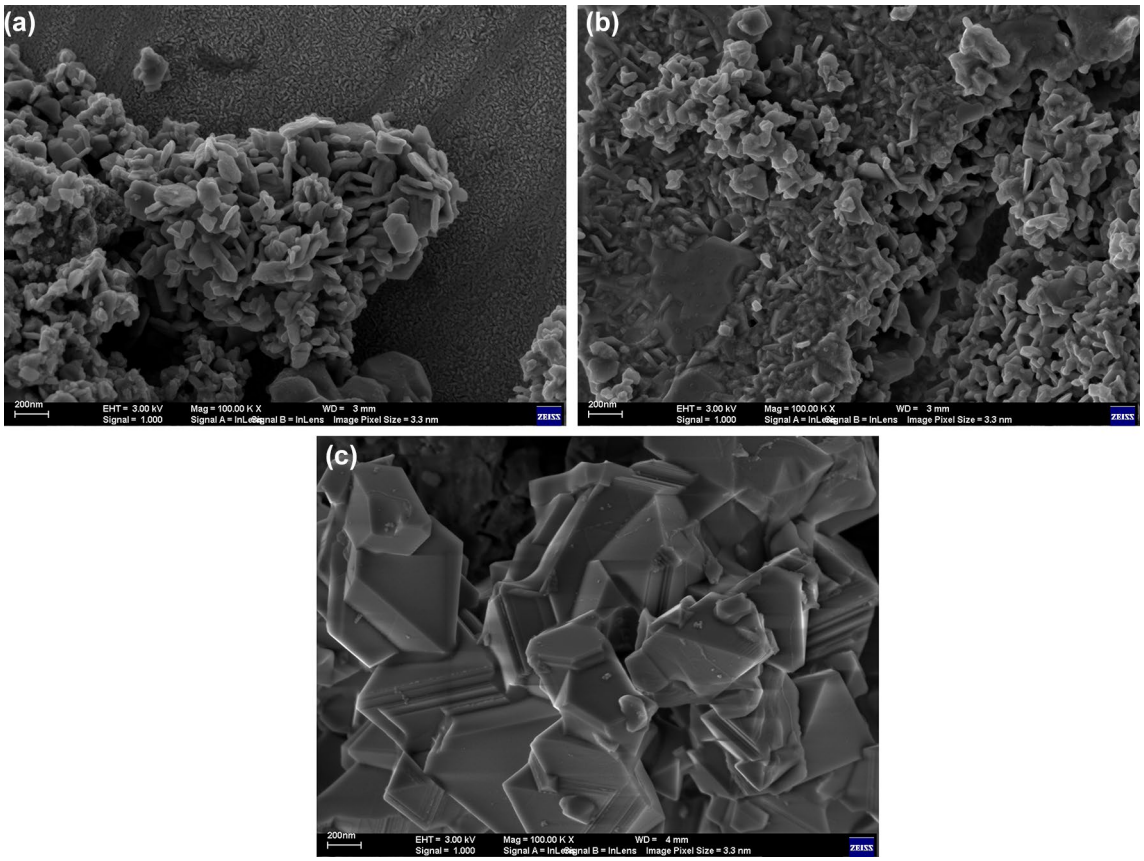

Fig. 4 FEG-SEM of $Y_3Fe_{3.35}Al_{1.65}O_{12}$ powders synthesized at 140 °C through microwave hydrothermal synthesis method with soaking times of: **a** 15, **b** 30 and **c** 60 min

soaking time in microwave (60 min) can cause damages in the magnetron of equipment. Therefore, 30 min seems to be the optimal time to obtain the garnet phase.

The temperature dependence of dielectric permittivity as a function of the soaking time at 10 kHz is shown in Fig. 7. For coarse-grained sample, the phase transition is observed at 337 K, and its maximum dielectric permittivity (ε_m) 15,760. A structural phase transition which corresponds to the transition of paraelectric to ferroelectric phase (at T_c) is observed. For medium- and fine-grained samples the same trend is noted. However, the maximum dielectric permittivity associated to phase transition temperature is reduced. The dielectric permittivity increases gradually with an increase in temperature up to the transition temperature (T_c), Curie point, and then decreases (Table 1). The temperature dependence of the dielectric permittivity at different soaking times shows that there is no dispersion at around Curie temperature. This should be explained by the relatively larger ionic radius of the B ions (Fe and Al) which enhances the thermal stability of the BO_6 octahedra. The phase transitions are around 64 °C. The region around the dielectric peak is broadened due to a disorder in the cations arrangement in one or more crystallographic sites of the structure. The reduction of dielectric permittivity indicates that Al^{3+} ions are doped into the YAG crystals, they gradually fill into the tetrahedrons and octahedrons and replace Fe^{3+} as their central ion. The magnitude of the dielectric permittivity decreases for high soaking times with no Curie temperature changes which indicates that dielectric polarization is a relaxation type in nature. The higher the soaking content, the disorder the Curie temperature because the number of the main magnetic interaction J_{ad} (where J_{ad} is the constant exchange between cations in a and d sites) per magnetic ion per formula was reduced. So in the composition range investigated, T_c values should be optimized allowing such particles self-regulated and safe-guarded for hyperthermia applications. To improve confiability, temperature-dependent magnetization curves and differential scanning calorimetry (DSC) should be performed. The Mössbauer spectra of the studied garnet obtained at 30 min is shown in the inset of Fig. 7. The results indicate that the iron is presented as Fe(III) only. The doublet components were constrained to be equal in width and intensity, and nearly overlapping peaks were easily resolved by the computer,

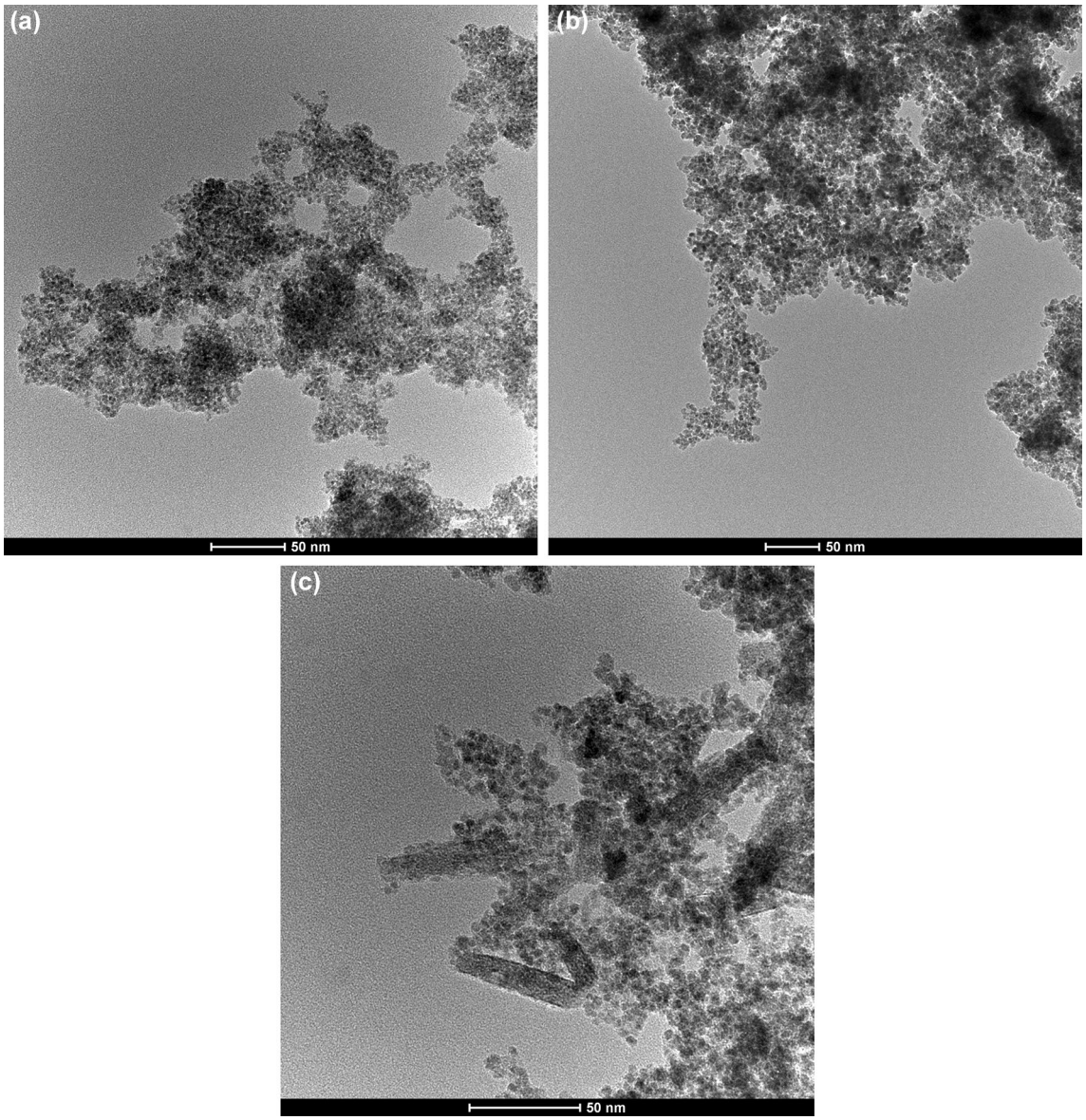

Fig. 5 TEM images of $Y_3Fe_{3.35}Al_{1.65}O_{12}$ powders synthesized at 140 °C through microwave hydrothermal synthesis method with soaking times of: **a** 15, **b** 30 and **c** 60 min

always converging to the same values despite different initial estimates. The resolved components do not exactly coincide, being separated by 0.27 mm s^{-1}. Two types of ion are seen in the YIG compounds, namely, with octahedral coordination and with close to tetrahedral coordination. According to the relative weight of the doublet lines, the ratio octa/tetra is 80/20. The differences between the determined parameters of the hyperfine interactions (isomer shift and quadrupole splitting) show that the introduction of Y leads to changes in the ligand field around Fe-ions, that is, the characteristics of the chemical bond and the electrical charge symmetry around the iron nucleus are slightly changed.

4 Conclusions

Microwave hydrothermal synthesis method allowed the formation of $Y_3Fe_{3.35}Al_{1.65}O_{12}$ nanoparticles at different soaking times, temperature of 140 °C and acid pH. Hydrothermal synthesis time is very important in crystalline network; it can change nanoparticles' formation and magnetic and dielectric properties. Agglomerates are formed

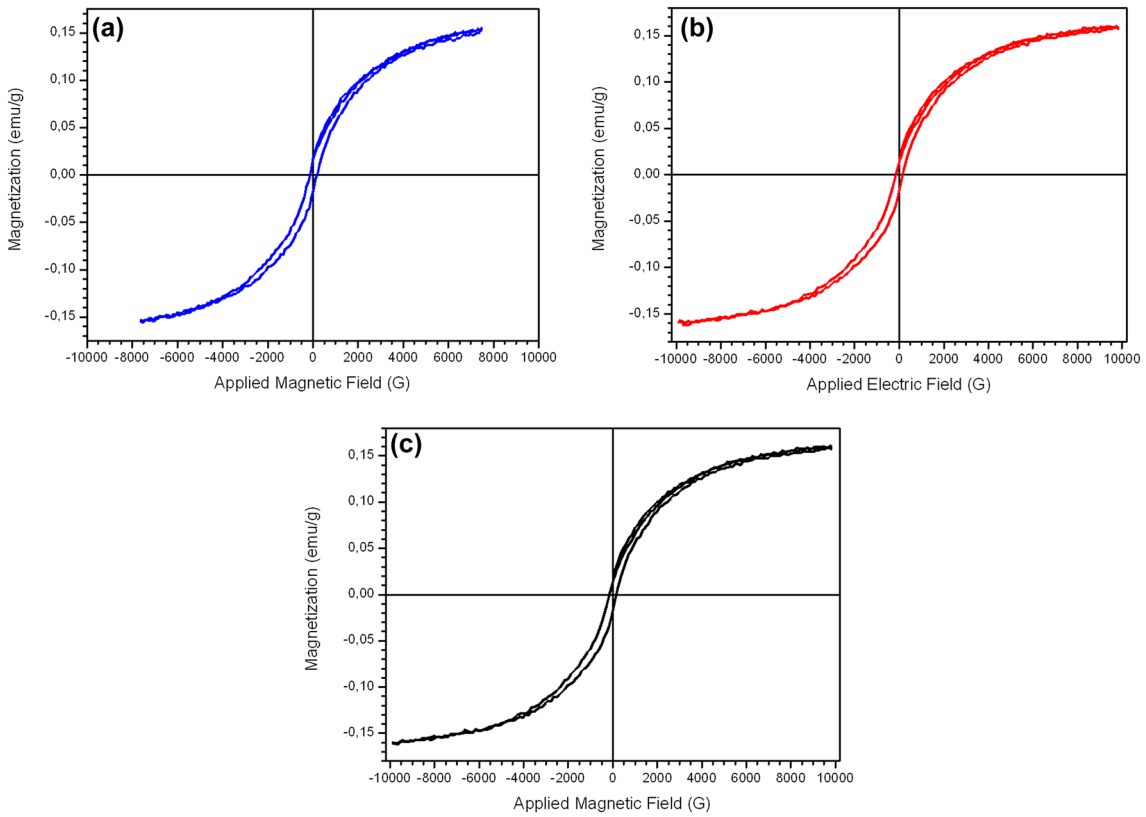

Fig. 6 M–H loops of $Y_3Fe_{3.35}Al_{1.65}O_{12}$ powders synthesized at 140 °C through microwave hydrothermal synthesis method with soaking times of 15, 30 and 60 min

Table 1 Particle size, permittivity and magnetic properties of $Y_3Fe_{3.35}Al_{1.65}O_{12}$ with soaking times of 15, 30 and 60 min

Samples	Particle size (nm)	ε_r	M_s (emu g^{-1})	M_r (emu g^{-1})	H_c (G)
15	26	14,566	0.1531	0.0169	189.521
30	38	15,140	0.1575	0.0150	154.139
60	60	15,760	0.1531	0.0134	153.363

for all soaking times with particle size reaching from 20 to 60 nm. Ferromagnetism was observed for all soaking times and saturation magnetization might be attributed to small volume of nanoparticles with high heat liberation. Soaking time of 30 min of crystallization showed similar remaining magnetization and low coercitive field than 15 min, greatest degree of regularity and most homogeneous morphology. The Mössbauer spectra of the studied garnet obtained at 30 min indicate that the iron is presented as Fe(III) only. In order to make these ferrites potential candidates for magneto hyperthermia applications using hydrothermal method it is necessary to reduce the Curie point near body temperature by adjusting Fe/Al ratio.

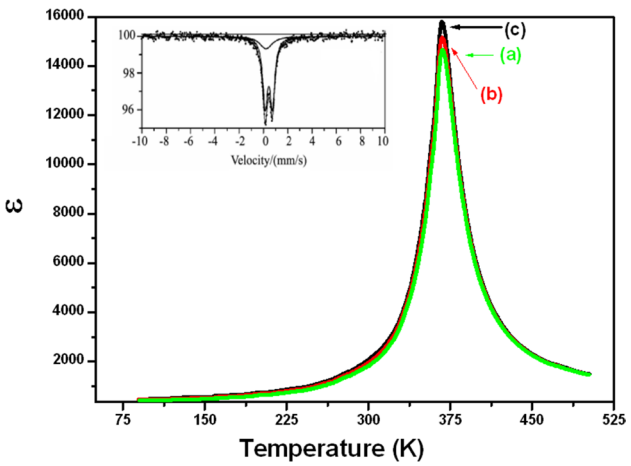

Fig. 7 Permittivity of $Y_3Fe_{3.35}Al_{1.65}O_{12}$ pellets as a function of temperature obtained through microwave hydrothermal synthesis method with soaking times of 15, 30 and 60 min. Inset shows the Moissbauer spectrum of $Y_3Fe_{3.35}Al_{1.65}O_{12}$ powders synthesized at 140 °C through microwave hydrothermal synthesis method with soaking time of 30 min fitted to one doublet assigned to Fe^{3+}

Acknowledgements The financial support of this research project by the Brazilian research funding agency FAPESP 2014/16993-1. The funding was supported by FAPESP (Grant No. 2013/07296-2).

References

1. P. Moroz, S.K. Jones, B.N. Gray, Magnetically mediated hyperthermia: current status and future directions. Int. J. Hyperth. **18**, 267–284 (2002)
2. J.J.W. Lagendijk, Hyperthermia treatment planning. Phys. Med. Biol. **45**, R61–R76 (2000)
3. A.R. Jordan, K. Scholz, M. Maier-Hauff, P. Johannsen, J. Wust, H. Nadobny, H. Schirra, S. Schmidt, S. Deger, W. Loening, R. Lanksch, Felix, Presentation of a new magnetic field therapy system for the treatment of human solid tumors with magnetic fluid hyperthermia. J. Magn. Magn. Mater. **225**, 118–126 (2001)
4. K. Maier-Hauff, R. Rothe, B. Thiesen, A. Jordan, Intracranial thermotherapy using magnetic nanoparticles combined with external beam radiotherapy: results of a feasibility study on patients with glioblastoma multiforme. J. Neurooncol. **81**, 53–60 (2007)
5. K. Maier-Hauff, R. Rothe, B. Thiesen, A. Jordan, H. Orawa, A. Jordan, Efficacy and safety of intratumoral thermotherapy using magnetic iron-oxide nanoparticles combined with external beam radiotherapy on patients with recurrent glioblastoma multiforme. J. Neurooncol. **103**, 317–324 (2011)
6. M. Johannsen, U. Gneveckow, B. Thiesen, N. Waldöfner, R. Scholz, S.A. Loening, P. Wust, Thermotherapy of prostate cancer using magnetic nanoparticles: feasibility, imaging, and three-dimensional temperature distribution. Eur. Urol. **52**, 1653–1662 (2007)
7. R.K. Gil Christian, R. Medal, W.D. Shorey, R.C. Hanselman, J.C. Parrot, C.B. Taylor, Selective inductive heating of lymph nodes. Ann Surg. **146**, 596–606 (1957)
8. V.F. Castro, J. Celestino, A.A.A. Queiroz, F.G. Garcia, Propriedades magnéticas e biocompatíveis de nanocompósitos para utilização em magneto-hipertermia, Rev. Bras. Fís. Méd. **4**, 79–82 (2010)
9. C.S.S.R. Kumar, F. Mohammad, Magnetic nanomaterials for hyperthermia-based therapy and controlled drug delivery. Adv. Drug Deliv. Rev. **63**, 789–808 (2011)
10. Z.A. Motlagh, M. Mozaffari, J. Amighian, Preparation of nanosized Al-substituted yttrium iron garnets by the mechanochemical method and investigation of their magnetic properties. J. Magn. Magn. Mater. **321**, 1980–1984 (2009)
11. F. Bertaut, O.F. Forrat, Structure des ferrites ferrimagnetiques des terres rares. Compt. Rend. **242**, 382–385 (1956)
12. Y.F. Chen, K.T. Wu, Y.D. Yao, C.H. Peng, W.S. Tse, The influence of Fe concentration on $Y_3Fe_{5-x}Al_xO_{12}$ garnets. Microelectron. Eng. **81**, 329–335 (2005)
13. M. Othman, M.F. Ain, N.S. Abdullah, Z.A. Ahmad, Studies on the formation of yttrium iron garnet (YIG) through stoichiometry modification prepared by conventional solid-state method. J. Eur. Ceram. Soc. **33**, 1317–1324 (2013)
14. Z. Cheng, H. Yang, Synthesis and magnetic properties of Sm–$Y_3Fe_5O_{12}$ nanoparticles. Physica E. **39**, 198–202 (2007)
15. Z.A. Motlagh, M. Mozaffari, J. Amighian, A.F. Lehlooh, M. Awawdeh, S. Mahmood, Mössbauer studies of $Y_3Fe_{5-x}Al_xO_{12}$ nanopowders prepared by mechanochemical method. Hyperfine Interact. **198**, 295–302 (2010)
16. M.N. Akhtar, M.A. Khan, S.F. Shaukat, M.H. Asif, N. Nasir, G. Abbas, Nazir, $Y_3Fe_5O_{12}$ nanoparticulate garnet ferrites: comprehensive study on the synthesis and characterization fabricated by various routes. J. Magn. Magn. Mater. **368**, 393–400 (2014)
17. R. Hergt, S. Dutz, R. Muller, M. Zeisberger, Magnetic particle hyperthermia: nanoparticle magnetism and materials development for cancer therapy. J. Phys. Condens. Matter. **18**, S2919–S2934 (2006)
18. M.N. Akhtar, M.A. Khan, M.R. Raza, M. Ahmad, S.F. Shaukat, M.H. Asif, M. Saleem, M.S. Nazir, Structural, morphological, dielectric and magnetic characterizations of $Ni_{0.6}Cu_{0.2}Zn_{0.2}Fe_2O_4$ (NCZF/MWCNTs/PVDF) nanocomposites for multilayer chip inductor (MLCI) applications. Ceram. Int. **40**, 15821–15829 (2014)
19. F. Grasset, S. Mornet, A. Demourgues, J. Portier, J. Bonnet, A. Vekris, E. Duguet, Synthesis, magnetic properties, surface modification and cytotoxicity evaluation of $Y_3Fe_{5-x}Al_xO_{12}$ ($0 \leq x \leq 2$) garnet submicron particles for biomedical applications. J. Magn. Magn. Mater. **234**, 409–418 (2001)
20. H. Yu, L. Zeng, C. Lu, W. Zhang, G. Xu, Synthesis of nanocrystalline yttrium iron garnet by low temperature solid state reaction. Mater. Charact. **62**, 378–381 (2011)
21. D.T.T. Nguyet, N.P. Duong, T. Satoh, L.N. Anh, T.D. Hien, Temperature-dependent magnetic properties of yttrium iron garnet nanoparticles prepared by citrate sol–gel. J. Alloy. Compd. **541**, 18–22 (2012)
22. Y.-P. Fu, C.-H. Lin, P. Ko-Ying, Microwave-induced combustion synthesis of yttrium iron garnet nano-powders and their characterizations. J. Magn. Magn. Mater. **272–276**, 2202–2204 (2004)
23. P. Grosseau, A. Bachiorrini, B. Guilhot, Preparation of polycrystalline yttrium iron garnet ceramics. J. Therm. Anal. **46**, 1633–1641 (1996)
24. P. Vaqueiro, M.A. Lopez-Quintela, J. Rivas, Synthesis of yttrium iron garnet nanoparticles via coprecipitation in microemulsion. J. Mater. Chem. **7**, 501–505 (1997)
25. S. Taketomi, Y. Ozaki, K. Kawasaki, S. Yuasa, A.H. Miyaiwa, Transparent magnetic fluid: preparation of YIG ultrafine particles. J. Magn. Magn. Mater. **122**, 6–10 (1993)
26. S. Komarneni, Q.H. Li, R. Roy, Microwave-hydrothermal processing for synthesis of layered and network phosphates. J. Mater. Chem. **4**, 1903–1906 (1994)
27. A.P. Alivisatos, Semiconductor clusters, nanocrystals, and quantum dots. Science **271**, 933–937 (1996)
28. Y. Cui, C.M. Lieber, Functional nanoscale electronic devices assembled using silicon nanowire buiding blocks. Science **291**, 851–853 (2001)
29. J.T. Hu, O.Y. Min, P.D. Yang, C.M. Lieber, Controlled growth and electrical properties of heterojunctions of carbon nanotubes and silicon nanowires. Nature **399**, 48–51 (1999)
30. E.W. Dai, H.J. Wong, Y.Z. Lu, S.S. Fan, C.M. Lieber, Synthesis and characterization of carbide nanorods. Nature **375**, 769–772 (1995)
31. A. Sobhani-Nasaba, M. Rahimi-Nasrabadi, H. RezaNaderi, V. Pourmohamadian, F. Ahmadi, M.R. Ganjali, H. Ehrlich, Sonochemical synthesis of terbium tungstate for developing high power supercapacitors with enhanced energy densities. Ultrason. Sonochem. **45**, 189–196 (2018)
32. E.-A. Mohammad, A. Sobhani-Nasabb, M. Rahimi-Nasrabadic, F. Ahmadid, S. Pourmasoud, Ultrasound-assisted synthesis of $YbVO_4$ nanostructure and $YbVO_4$/$CuWO_4$ nanocomposites for enhanced photocatalytic degradation of organic dyes under visible light. Ultrason. Sonochem. **43**, 120–135 (2018)
33. M. Rahimi-Nasrabadi, F. Ahmadi, Investigation of optical properties and the photocatalytic activity of synthesized $YbYO_4$

nanoparticles and $YbVO_4/NiWO_4$ nanocomposites by polymeric capping agents. J. Mol. Struct. **1157**, 607–615 (2018)
34. M. Salavati-Niasari, F. Soofivand, A. Sobhani-Nasab, M. Shakouri-Arani, M. Hamadanian, S. Bagheri, M. Hamadanian, S. Bagheri, Facile synthesis and characterization of $CdTiO_3$ nanoparticles by Pechini sol-gel. J. Mater. Sci. Mater. Electron. **28**, 14965–14973 (2017)
35. D.V.M. Paiva, M.A.S. Silva, T.S. Ribeiro, I.F. Vasconcelos, A.S.B. Sombra, P.B.A. Fechine, Novel magnetic-dielectric composite ceramic obtained from $Y_3Fe_5O_{12}$ and $CaTiO_3$. J. Alloy. Compd. **644**, 763–769 (2015)